Optical and Quantum Electronics

Generation of an ultrabroadband supercontinuum in the mid-infrared region using dispersion-engineered GeAsSe photonic crystal fiber

--Manuscript Draft--

Manuscript Number:	
Full Title:	Generation of an ultrabroadband supercontinuum in the mid-infrared region using dispersion-engineered GeAsSe photonic crystal fiber
Article Type:	Original Research
Keywords:	Numerical analysis and approximation; Microstructured fiber; Ultrafast nonlinear optics; Chalcogenide; Supercontinuum generation
Corresponding Author:	Harith b Ahmad, PhD Photonics Research Centre, University of Malaya Kuala Lumpur, MALAYSIA
Corresponding Author Secondary Information:	
Corresponding Author's Institution:	Photonics Research Centre, University of Malaya
Corresponding Author's Secondary Institution:	
First Author:	Harith b Ahmad, PhD
First Author Secondary Information:	
Order of Authors:	Harith b Ahmad, PhD
	Mohammad Karim
	Souvik Ghosh
	Aziz Rahman
Order of Authors Secondary Information:	
Funding Information:	Ministry of Higher Education, Malaysia (GA 010-2014 (ULUNG)) — Dr. Harith b Ahmad
	Universiti Malaya (RP029B-15 AFR and RU001-2017) — Dr. Harith b Ahmad
	Newton Fund (IF026-2018) — Dr. Harith b Ahmad
Abstract:	An ultrabroadband mid-infrared (MIR) region supercontinuum (SC) generation is demonstrated numerically through dispersion-engineered traditional chalcogenide (ChG) photonic crystal fiber (PCF). By varying structural parameters pitch (hole to hole spacing) and air-hole diameter to pitch ratio, a number of 10-mm-long hexagonal PCFs made employing GeAsSe ChG glass as a core and air-holes of hexagonal lattice running through their lengths as a cladding are optimized to predict an efficient mid-infrared region SC spectral emission by pumping them using a tunable pump source between 2.9 μm and 3.3 μm. Simulations are carried out using an ultrashort pump pulse of 100-fs duration with a low pulse peak power between 3 kW and 4 kW into the optimized designs. It is found through numerical analysis that the efficient SC spectral broadening with flattened output can be obtained by increasing the PCF pitch rather than increasing the PCF cladding containing air-hole diameter although it could able to be obtained a larger nonlinear coefficient through increasing air-hole diameter of an optimized design. Simulation results show that the SC spectra can be broadened up to 12.2 μm for a certain design with a peak power of 3 kW. Using a peak power of 4 kW, it is possible to obtain SC spectral broadening beyond 14 μm with an optimized design spanning the wavelength range from 1.8 to 14 μm which covers the electromagnetic spectrum required for MIR molecular fingerprint region applications such as sensing and biological imaging.

Noname manuscript No.
(will be inserted by the editor)

Generation of an ultrabroadband supercontinuum in the mid-infrared region using dispersion-engineered GeAsSe photonic crystal fiber

H. Ahmad[1,2] · **M. R. Karim**[1] · **Souvik Ghosh**[3] · **B. M. A. Rahman**[3]

the date of receipt and acceptance should be inserted later

Abstract An ultrabroadband mid-infrared (MIR) region supercontinuum (SC) generation is demonstrated numerically through dispersion-engineered traditional chalcogenide (ChG) photonic crystal fiber (PCF). By varying structural parameters pitch (hole to hole spacing) and air-hole diameter to pitch ratio, a number of 10-mm-long hexagonal PCFs made employing GeAsSe ChG glass as a core and air-holes of hexagonal lattice running through their lengths as a cladding are optimized to predict an efficient mid-infrared region SC spectral emission by pumping them using a tunable pump source between 2.9 μm and 3.3 μm. Simulations are carried out using an ultrashort pump pulse of 100-fs duration with a low pulse peak power between 3 kW and 4 kW into the optimized designs. It is found through numerical analysis that the efficient SC spectral broadening with flattened output can be obtained by increasing the PCF pitch rather than increasing the PCF cladding containing air-hole diameter although it could able to be obtained a larger nonlinear coefficient through increasing air-hole diameter of an optimized design. Simulation results show that the SC spectra can be broadened up to 12.2 μm for a certain design with a peak power of 3 kW. Using a peak power of 4 kW, it is possible to obtain SC spectral broadening beyond 14 μm with an optimized design spanning the wavelength range from 1.8 to 14 μm which covers the electromagnetic spectrum required for MIR molecular fingerprint region applications such as sensing and biological imaging.

H. Ahmad
E-mail: harith@um.edu.my

[1]Photonics Research Centre, Faculty of Science, University of Malaya, 50603 Kuala Lumpur, Malaysia

[2]Visiting Professor at the Department of Physics, Faculty of Science and Technology, Airlangga University, Surabaya 60115, Indonesia

[3]Department of Electrical and Electronic Engineering, City University of London, Northampton Square, London, EC1V 0HB, UK

Keywords Numerical analysis and approximation · Microstructured fiber · Ultrafast nonlinear optics · Chalcogenide · Supercontinuum generation

1 Introduction

Supercontinuum (SC) generation using microstructured fibers has drawn considerable attention in last decade owing to its manifold applications which include biomedical imaging, high-resolution spectroscopy, optical coherence tomography, high precision frequency metrology, gas sensing and food quality control (Petersen et al. 2014). More specifically, recently SC sources designed using microstructured and tapered fibers which provide a high brightness and high resolution broadband light source for the applications in early cancer detection using optical biopsy (Seddon et al. 2016), hyper-spectral infrared microscopy (Dupont et al. 2012), multispectral tissue imaging (Petersen et al. 2018) and optical biosensing (Markos et al. 2015). Microstructured fibers usually become highly nonlinear owing to the nature of their structural formations and widely used powerful fiber technology method for designing high brightness broadband SC sources between ultraviolet and mid-infrared region applications (Dudley et al. 2009). Among different microstructured fiber based designs, photonic crystal fiber (PCF) is the most prominent design due to its flexible design procedure which is possible through the variation of its two structural parameters pitch and hole-diameter (Knight et al. 1996; Cregan el al. 1999; Knight et al. 2002; Tajima et al. 2004; Fatome et al. 2009). To achieve broadband SC spectral evolution, optical waveguide usually requires to pump using ultrashort optical pulses in anomalous group velocity dispersion (GVD) regime (Agrawal 2013). Controlled GVD optimization of a waveguide geometry over a wide wavelength range in both the anomalous and normal dispersion regions as well as GVD parameter in a certain wavelength vicinity to the existing pump sources can comfortably be achieved through the variation of PCF geometrical parameters (Dudley et al. 2006).

Nowadays, researchers are focusing on mid-infrared (MIR) region SC generation (2–20 μm) which belongs to two most important transparent windows such as 3–5 μm and 8–13 μm that can be used to detect the scent of different toxic gases which are detrimental to the various environmental and atmospheric applications (Schliesser et al. 2012). To extend the SC spectral evolution up to this limit, several host materials with various designs have been proposed to push the long wavelength side of SC extension far into the MIR region. Among those materials, fluoride (Qin et al. 2009; Swiderski et al. 2014), tellurite (Liao et al. 2011; Cheng et al. 2015; Domachuk et al. 2008) and ChG glasses (Gai et al. 2010; Hudson et al. 2012; Magi et al. 2007; Al-Kadry et al. 2014; Kubat et al. 2014; Eggleton et al. 2011; Aggarwal et al. 2002; Ma et al. 2013; Shaw et al. 2011; Hu et al. 2010; Møller et al. 2015; Gao et al. 2013; Yu et al. 2015; Karim et al. 2015) with wider transparency and high Kerr nonlinearity have been studied extensively for MIR region SC generation. Fluoride and tellurite glasses have transparency up to 5 μm, however, the transparency of ChG glasses can be extended between 10 μm and 20 μm depending on the chemical composition used during fabrication. Moreover, high refractive index, large Kerr nonlinearity (n_2) and low two-photon absorption (TPA) due to moderate band-gap around the telecommunication wavelength of

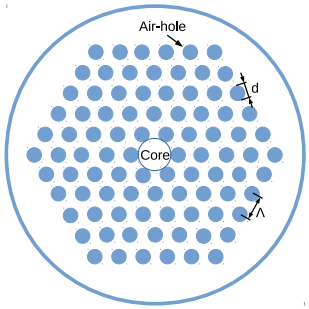

Fig. 1 ChG PCF geometry for dispersion optimization.

ChG glasses make them most suitable host materials for MIR region SC generation (Sanghera et al. 2008; Wei et al. 2013).

Some recent theoretical and experimental demonstrations of MIR SC generation through ChG step-index and microstructured fibers are mentioned below (Karim et al. 2018; Saini et al. 2015; Ou et al. 2016; Cheng et al. 2016; Zhao et al. 2017; Petersen et al. 2017; Hudson et al. 2017). Karim *et al.* (Karim et al. 2018) recently numerically reported ultrabroadband MIR SC generation covering the wavelength range 2.3–15 μm using a 10-mm-long all-ChG triangular core microstructured fiber (GeAsSe/GeAsS) when pumped at 4 μm with a pulse duration of 100-fs and a low peak power of 3 kW while Saini *et al.* (Saini et al. 2015) numerically demonstrated MIR SC spectral evolution extending up to 15 μm in a 5-mm long triangular core graded index As_2Se_3 microstructured fiber using pump at 4.1 μm with an input peak power of 3.5 kW. Ou *et al.* (Ou et al. 2016) demonstrated an ultrabroadband SC generation in the MIR region up to 14 μm with a 20-cm-long ChG step-index fiber using $Ge_{15}Sb_{25}Se_{60}$ glass as the core and $Ge_{12}Sb_{20}Se_{65}$ glass for its cladding when pumped with a 150-fs pulse duration at 6 μm and a peak power of 750 kW. Cheng *et al.* (Cheng et al. 2016) reported a MIR SC spanning the wavelength range 2-15.1 μm in a 3-cm-long ChG step-index fiber employing As_2Se_3 for its core and $AsSe_2$ for its outer cladding pumped with a 170-fs pulses in 9.8 μm with a peak power of 2.89 MW. Zhao *et al.* (Zhao et al. 2017) reported a MIR SC spectral evolution spanning up to 16 μm using a 14-cm-long step-index fiber fabricated from Ge-Te-AgI glass when pumped with 150-fs pulses at 7 μm having a pulse repetition rate of 1 kHz with a peak power of 77 W. Petersen *et al.* (Petersen et al. 2017) reported a MIR SC spectral broadening spanning from 1 to 11.5 μm with high average output power in tapered large-mode-area ChG $Ge_{11}As_{22}Se_{68}$ photonic crystal fiber. Hudson *et al.* (Hudson et al. 2017) reported an ultrabroadband MIR region SC generation covering from 1.8 to 9.5 μm employing As_2Se_3/As_2S_3 tapered fiber by launching 230-fs pulses with a pulse peak power of 4.2 kW. For a broadband SC generation, recently developed hollow-core band-gap guiding hybrid PCFs have also attracted considerable attention due to their inherent ability to integrate with different fluids, solids, and gases which can significantly extend the functionality of these fibers due to easier tunning of dispersion and nonlinearity (Markos et al. 2017; Habib et al. 2017).

In this numerical study, we optimized a number of 10-mm-long typical hexagonal PCFs by employing $Ge_{11.5}As_{24}Se_{64.5}$ ChG glass for their cores and the air-holes running for their outer claddings throughout the length of the fibers. Among

all ChG chemical compositions, $Ge_{11.5}As_{24}Se_{64.5}$ ChG glass has a transparency up to 14 μm. By varying structural parameters, all the PCFs are optimized for pumping them between 2.9 μm and 3.3 μm using a tunable pump source in the anomalous dispersion regime and the pump wavelength of each design is selected vicinity to the zero-dispersion wavelength (ZDW). Simulations are carried out using 100-fs duration pump pulses with a low peak powers between 3 kW and 4 kW into the optimized PCF geometries. The MIR region SC spectral broadening has been reached up to the transparency limit ($\sim$14 μm) of the ChG material proposed by one of the optimized design.

2 Theory

A typical hexagonal PCF as shown in Fig. 1 is proposed for our modeling which can be made from $Ge_{11.5}As_{24}Se_{64.5}$ ChG glass core and its outer cladding comprised of air-holes running through the fiber length. To keep confinement (leakage) losses minimum, five air-holes rings are considered during modal analysis of the proposed PCF structures. The frequency dependent linear refractive index data can be evaluated over a wide frequency range from the Sellmeier polynomial proposed by Ma *et al.* (Ma et al. 2013). The ChG PCFs are modeled and optimized by varying their pitch (Λ) and air-hole diameter to pitch ratio (d/Λ) through our computer code which is developed by using finite-element method (FEM) (Rahman and Davis 1984). In order to obtain high accuracy modal solution through FEM mode-solver, only one-quarter of PCF geometry is simulated in transverse directions using 720,000 first-order triangular elements through exploiting its two-fold symmetry which eventually allows to use more dense mesh distribution in a quarter area instead of a whole PCF geometry. To calculate the proposed PCFs confinement loss, perfectly matched layer (PML) is placed at the boundary of the geometry. In order to optimize a PCF geometry for pumping it using a tunable pump source with wider anomalous dispersion, its two structural parameters Λ and d/Λ are varied during FEM simulation to evaluate the mode propagation constant (β) of fundamental mode (H_x^{11}) which is later utilized to evaluate the GVD parameter over a wide wavelength range. The proposed PCF structure shows slight birefringence due to its six fold symmetry. The β for the other polarization, H_y^{11} is evaluated through FEM simulations and the GVD parameters are calculated using this β up to the wavelength range of interest. No significant differences are obtained between GVD values achieved from two different polarizations.

By launching short optical pulses vicinity to the zero-dispersion wavelength (ZDW) in the anomalous GVD region, the SC spectral evolution inside the optimized ChG PCF structure can be studied through the widely used generalized nonlinear Schrödinger equation (GNLSE) (Agrawal et al. 2013) including two-photon absorption (TPA) into it (Karim et al. 2014):

$$\frac{\partial}{\partial z}A(z,T) = -\frac{\alpha}{2}A + \sum_{r\geq 2}^{16}\frac{i^{r+1}}{r!}\beta_r\frac{\partial^r A}{\partial T^r} + i\left(\gamma + i\frac{\alpha_{\mathrm{TPA}}}{2A_{\mathrm{eff}}}\right)\left(1 + \frac{i}{\omega_0}\frac{\partial}{\partial T}\right) \times \left(A(z,T)\int_{-\infty}^{\infty} R(T) \mid A(z,T-T') \mid^2 dT'\right), \quad (1)$$

where the electric-field envelope, $A(z,T)$ moves with the group velocity $1/\beta_1$ in a retarded frame $T = t - \beta_1 z$, β_r $(r \geq 2)$ is the r^{th} order dispersion parameter. γ is a nonlinear parameter which defines as $\gamma = n_2\omega_0/(cA_{\text{eff}}(\omega))$, where n_2 is the Kerr nonlinearity at pump frequency ω_0, c represents the velocity of light, and A_{eff} is the frequency dependent effective mode area. The linear propagation attenuation is added through α and the nonlinear absorption loss, TPA is added through $\alpha_{\text{TPA}} = 7.88 \times 10^{-14}$ m/W (Wang et al. 2014).

Intrapulse Raman scattering plays a vital role during SC generation and the response function of it can be represented by (Agrawal et al. 2013)

$$R(t) = (1 - f_{\text{R}})\delta(t) + f_{\text{R}}h_{\text{R(t)}}, \tag{2}$$

where instantaneous electronic and delayed Raman contributions are included.

The Raman contributions can be expressed as (Agrawal et al. 2013)

$$h_{\text{R(t)}} = \frac{\tau_1^2 + \tau_2^2}{\tau_1\tau_2^2} \exp\left(-\frac{t}{\tau_2}\right) \sin\left(\frac{t}{\tau_1}\right). \tag{3}$$

Here, the single-peak Lorentz function coefficients, $f_{\text{R}} = 0.148$, $\tau_1 = 23$-fs, and $\tau_2 = 164.5$-fs of As_2Se_3 material (Liu et al. 2016) are used to model the Raman response of GeAsSe material.

3 Numerical Results

In order to achieve wideband SC spectral evolution extending up to the MIR, the PCF geometry fabricated based on hexagonal lattice is very popular among researchers as this kind of structure has the ability to offer strong light confinement inside the core, which yields a larger nonlinear coefficient than any other fiber based design. This becomes possible only due to the microstructuring mechanism that is applied on the PCF's cladding containing air-holes. Flat GVD with smaller magnitude over wide wavelength range, which is the another vital factor acting behind the large SC spectral broadening, can be achieved using this mechanism

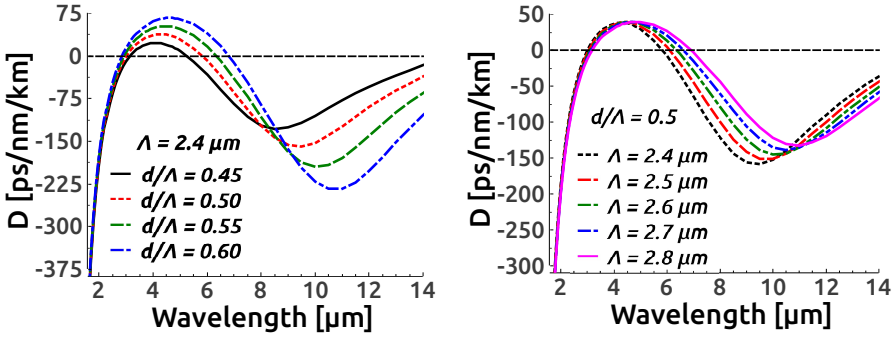

(a) (b)

Fig. 2 GVD curves optimized for ChG PCF by varying (a) d/Λ between 0.45 and 0.6 with a step of 0.05 keeping Λ constant at 2.4 μm and (b) Λ between 2.4 μm and 2.8 μm with a step of 0.1 μm keeping d/Λ constant at 0.5 for pumping the optimized structures between 2.9 μm and 3.3 μm.

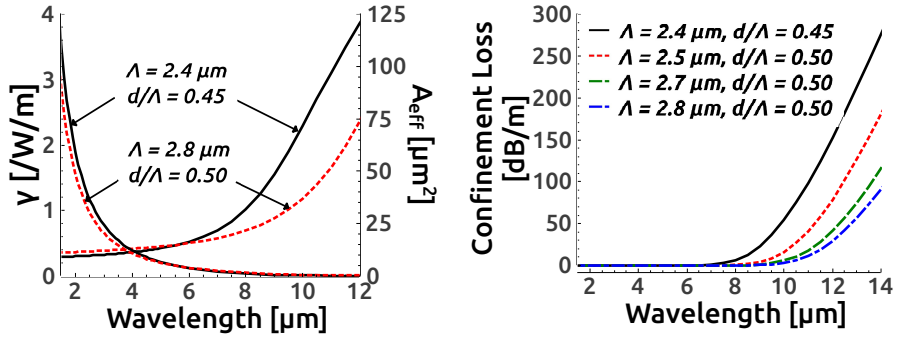

(a) (b)

Fig. 3 The mode effective areas of the PCF geometries $\Lambda = 2.4$ μm, $d/\Lambda = 0.45$ and $\Lambda = 2.8$ μm, $d/\Lambda = 0.5$ and their corresponding nonlinear coefficients are calculated in (a), and their confinement losses are shown over wide wavelength range in (b).

as well. For the proposed PCF designs, two sets of GVD curves are tailored by varying PCF structural parameters Λ and d/Λ for pumping them between 2.9 μm and 3.3 μm. By varying the ratio of d/Λ from 0.45 to 0.6 with a step of 0.05, first four designs are optimized whose Λ keeping fixed at 2.4 μm. The core diameter (2Λ–d) for these designs are calculated as 3.72 μm, 3.60 μm, 3.48 μm and 3.36 μm, respectively. Next, four designs are optimized by varying Λ between 2.5 μm and 2.8 μm while keeping d/Λ constant at 0.5 and the core diameters are calculated as 3.75 μm, 3.90 μm, 4.05 μm and 4.20 μm for these designs. To avoid fabrication difficulty of the design, the proposed PCFs are optimized by keeping d/Λ ratio below 0.7 (Xing et al. 2016). Figure 1 shows the tailored GVD curves for the optimized PCF designs. Two ZDWs are observed in each GVD curve and third ZDW can also be observed beyond 14 μm (not shown here). The position of ZDW of each GVD curves is varied with the variation of the PCF geometrical parameters. Between two structural parameters of PCF, it can be observed from figure that d/Λ variation is more sensitive than Λ variation in GVD optimization. For a small variation of d/Λ, it can be obsreved a large variation of GVD slope as well as a large variation of anomalous dispersion region in Fig. 2(a). However, in case of Λ variation, it is observed comparatively a smaller change of anomalous dispersion region while maintaining GVD slope nearly constant in Fig. 2(b). It is worth noting that the proposed design supports multimode propagation inside the PCF. Kubat *et al.* (Kubat et. al. 2016) shows that the SC bandwidth at the waveguide output would remain unaltered for the pump pulse duration of shorter than 10 ps in a multimoded fiber owing to the temporal walk-off. Raman induced power transfer between modes may not occur due to the short pump pulse duration. Thus, the SC bandwidth will not be affected at output of the PCF structure by the higher-order modes since it is considered here an ultra-short pump pulse with 100-fs duration for the all proposed designs.

For SC simulations, GNLSE Eq. (1) has been solved through symmetrized split-step Fourier method (Agrawal 2013) using MATLAB. Simulations are performed by taking 2^{17} grid points so that the time window can accommodate extreme spectral broadening inside it and to avoid negative frequency generation in the frequency grid, a minimum temporal resolution of 5.18-fs is considered. All SC

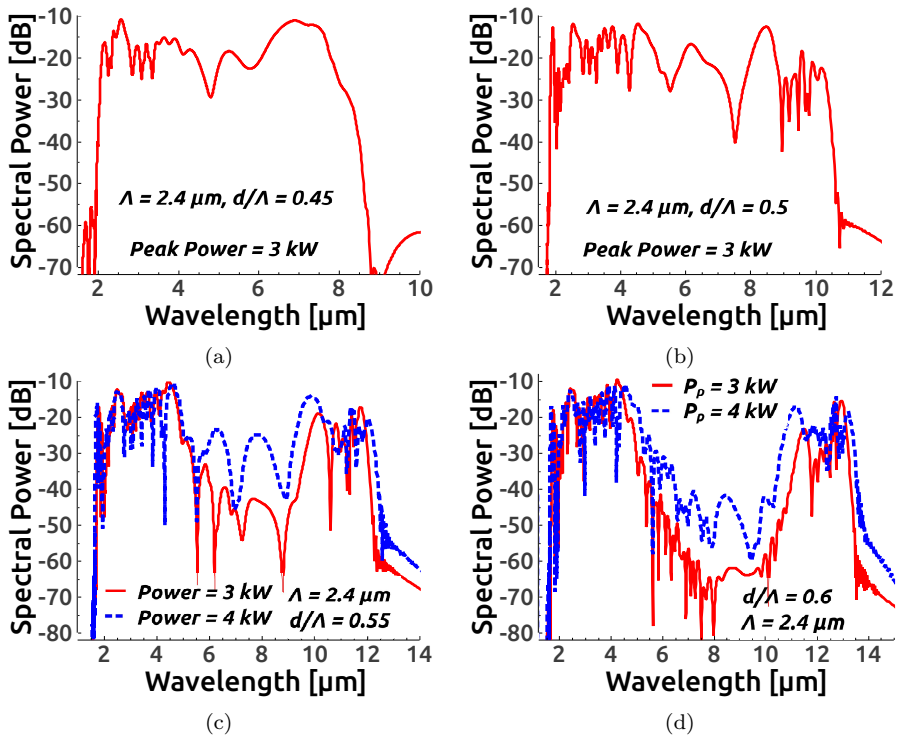

Fig. 4 SC spectral evolution in a 10-mm-long ChG PCF (dimensional parameters and peak powers as indicated inside the figure) pumped at (a) 3.2 μm; (b) 3.1 μm; (c) 3 μm; and (d) 2.9 μm using 100-fs pulses.

simulations are carried out using 100,000 axial steps with a step size of 100 nm in the pulse propagation direction. Since the higher-order dispersion terms play a significant role in the process of SC generation inside the optical waveguide and the inclusion of inadequate number of higher-order dispersion terms during SC simulation can lead to a spurious spectral broadening at the waveguide output, up to sixteenth-order higher-order terms (β_{16}) are calculated from the GVD curves illustrated in Fig. 2 and included them into GNLSE Eq. (1) during all SC simulations. A more conservative average material absorption loss, $\alpha = 0.5$ dB/cm is considered in comapred to the absorption loss reported in (Toupin et al. 2012; Xing et al. 2016; Xing et al. 2017) for the proposed GeAsSe material throughout all SC simulations. Mode effective areas are obtained through FEM mode-solver and their corresponding nonlinear coefficients (γ) are calculated using n_2 of 7.33 $\times$ 10^{-18} m^2/W (Wang et al. 2014) which are shown Fig. 3(a). Fig. 3(b) shows the confinement losses obtained through FEM mode-solver employing perfectly matched layer (PML) surrounding to the PCF computational domain. The ultrashort pulses with 100-fs duration tunable Raman soliton fluoride fiber laser pump source with a tunning range between 2 and 4.3 μm, which is reported by Tang *et al.* (Tang et al. 2016), is chosen to use as a pump source in all numerical simulations for SC generation.

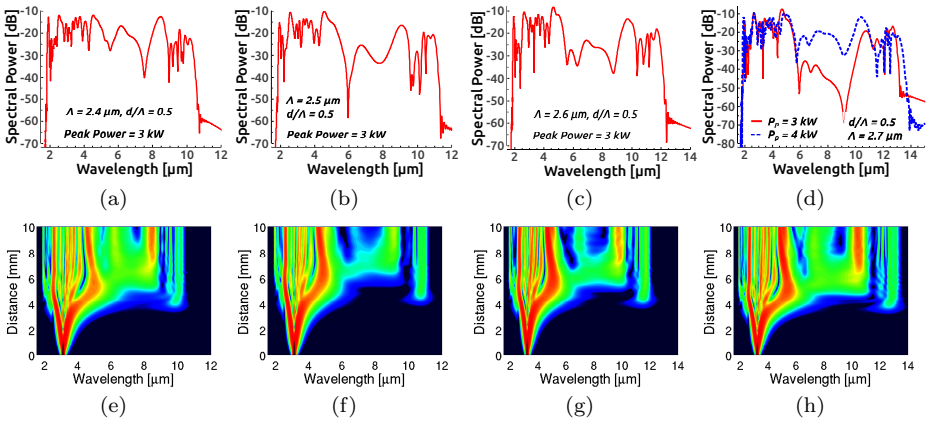

Fig. 5 SC spectral evolution in a 10-mm-long ChG PCF (dimensional parameters and input peak power as indicated inside the figure) pumped at (a) & (b) 3.1 μm; (c) & (d) 3.2 μm using 100-fs pulses and their corresponding spectral density evolutions are shown in (e)-(h), respectively. Spectral density evolutions (e)-(g) and (h) are plotted at a peak power of 3 kW and 4 kW, respectively.

For observing MIR SC spectral evolution, initially, four PCF geometries are optimized for pumping them with comparatively smaller GVD values close to the 1st ZDWs of the dispersion curves by varying d/Λ between 0.45 and 0.5 while keeping other structural parameter Λ constant at 2.4 μm. The GVD curves for the optimized structures are shown in Fig. 1(a) and the GVD value, D for these four PCF geometries at pump wavelengths of 3.2 μm, 3.1 μm, 3 μm and 2.9 μm are calculated as 2.41 ps/nm/km, 5.49 ps/nm/km, 6.19 ps/nm/km and 5.01 ps/nm/km, respectively. Utilizing the tunable pump source which can be tuned between 2 μm and 4.3 μm, the SC simulations are carried out using a sech pulse of 100-fs duration into the optimized structures with a low peak power between 3 kW and 4 kW. Figure 3 shows the MIR SC spectral output in four proposed designs (all red color curve for 3 kW and dashed blue curve for 4 kW peak power). Spectral broadening between 8.5 μm and 10.2 μm could be obtained with a peak power of 3 kW at a level of -20 dB from the peak for the PCF structures having d/Λ between 0.45 and 0.5 with Λ = 2.4 μm which can be seen in Fig. 4(a) and 4(b), respectively. It can be observed from Fig. 4(c) and 4(d) that spectral expansion can be extended between 12 and 13.5 μm with the same peak power at a level of -20 dB from the peak for the PCF geometries having d/Λ between 0.55 and 0.6. However, a spectral dip starts to appear if PCF optimizes with d/Λ = 0.55 and onwards with a low peak power of 3 kW. Thus, by increasing power to 4 kW, dip region can be improved (flatten out) as shown in Fig. 4(c) (dashed-blue line) for the structure having d/Λ ratio at 0.55. In case of PCF geometry having d/Λ = 0.6, spectra does not flattening out much as shown in Fig. 4(d) (dashed-blue line) with the same peak power applied and more peak power would be required to reach in the similar power level as compared to the earlier design.

To observe the Λ variation in the SC spectral evolution, next four PCF structures are optimized with the variations of Λ from 2.4 μm to 2.7 μm while keeping d/Λ value fixed at 0.5. D calculated for these structures at pump wavelength are 5.49 ps/nm/km, 2.31 ps/nm/km, 5.66 ps/nm/km and 5.83 ps/nm/km, re-

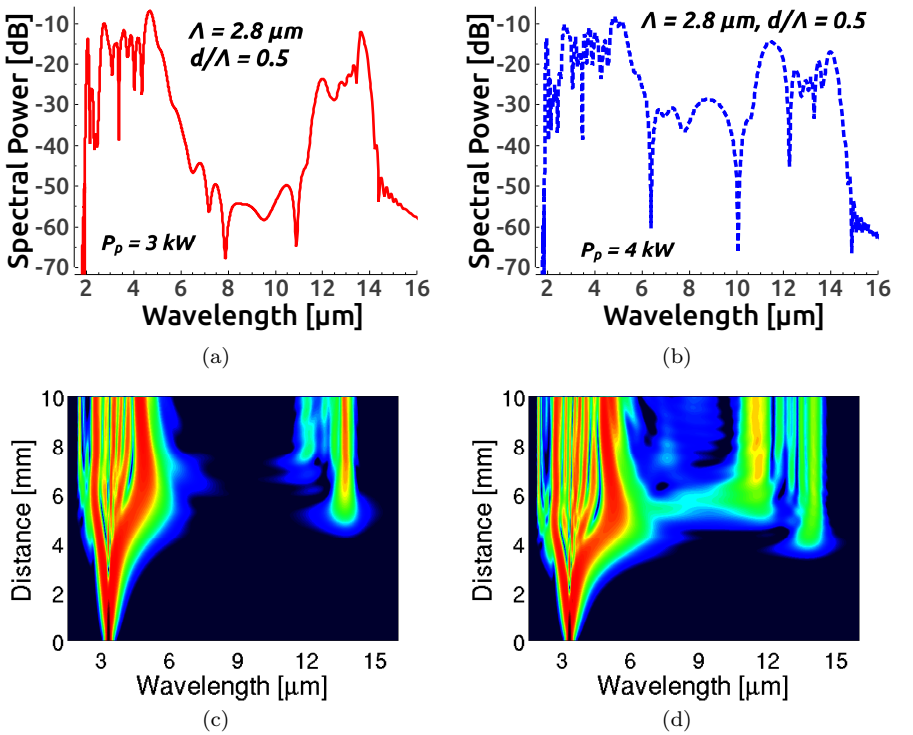

Fig. 6 SC spectral evolution in a 10-mm-long ChG PCF (dimensional parameters as indicated inside the figure) pumped at 3.3 μm using 100-fs pulses with an input peak power applied between 3 kW and 4 kW.

spectively. Figure 5 shows the SC spectral evolution for four different geometries optimized in two different pump wavelengths of 3.1 μm and 3.2 μm, respectively. MIR spectral spanning up to 10.2 μm could be realized for the PCF structure containing $\Lambda = 2.4$ μm that can be observed from Figs. 5(a) and 5(e). Subsequent enhanced spectra can be seen from the next three PCF geometries where the highest spectral extension is reached beyond 13 μm for the structure having a pitch length, $\Lambda = 2.7$ μm. For this structure, a small dip appears among the spectral components belong to the spectrum between 6 μm and 10 μm. Raising input peak power from 3 kW to 4 kW, spectral expansion can be realized up to 13.5 μm and the spectral dip can significantly be flattened as can be seen in Fig. 5(d) (dashed-blue line). Thus, we have observed in Λ variations of PCF geometry that it is possible to predict MIR region SC spectral evolution up to 12.2 μm (-30 dB level from the the peak) with a low peak power of 3 kW without inducing a dip by considering the largest Λ at 2.6 μm while keeping d/Λ constant at 0.5. Further increasing Λ to 2.7 μm induces a spectral dip with a peak power of 3 kW and more input peak power is required to obtain the similar spectral power level as compared to the earlier design.

To achieve spectral broadening beyond 14 μm up to the material transparency limit, one more PCF structure is optimized for pumping it at 3.3 μm wavelength by considering $\Lambda = 2.8$ μm while keeping the d/Λ value as same as before. The

Table 1 Output SC BW ranges predicted for various PCF geometries optimized

PCF Parameters		Input Peak Power	BW range
Λ [μm]	d/Λ	[kW]	[μm]
2.4	0.45		2.0–8.5
2.4	0.50		1.8–10.2
2.4	0.55		1.8–12.0
2.4	0.60	3	1.8–13.5
2.5	0.50		1.8–11.5
2.6	0.50		1.8–12.2
2.7	0.50	4	1.8–13.5
2.8	0.50		1.8–14.2

GVD, D evaluated for this structure at a pump wavelength is 5.83 ps/nm/km. After carrying out numerical simulation into this final optimized structure, the SC spectral broadening beyond 14 μm could be observed which can be clearly seen in Figs. 6(a) and 6(c) where a spectral dip appears between 7 μm and 11 μm with a peak power of 3 kW. In this case, the SC spectrum extends up to 14 μm, however, more power depletion occurs at the middle of the spectrum than that of the earlier design. By increasing peak power from 3 kW to 4 kW while keeping all other parameters same, another SC simulation for the same PCF structure is carried out and its corresponding simulation results are illustrated in Figs. 6(b) and 6(d). Although spectral broadening extends beyond 14 μm, still dip remains despite the peak power enhanced up to 4 kW. Another alternative way to spanning the SC spectra beyond 14 μm by changing or shifting the current pump source beyond 3.3 μm. In that case, the PCF geometries have to be optimized by increasing their Λ beyond 2.8 μm which will definitely induce more power depletion at the middle of the spectrum which eventually requires more input peak power to flatten out the dip. On the other hand, one can ask about what may happen if we enhance the other PCF parameter d/Λ during optimization. It is already observed that the PCF optimizes by increasing d/Λ ratio more than 0.5 would give us broad anomalous dispersion region GVD curve with a larger GVD slope which eventually does not extend the spectrum similar to a lower slope design. Nevertheless, keeping the input peak power at 4 kW with a tunning pump source and keeping the length of Λ between 2.7 μm and 2.8 μm while maintaining d/Λ ratio at 0.5, it could be possible to extend the SC spectrum up to 14 μm. Table I illustrated the MIR SC bandwidth (BW) ranges at the proposed ChG PCFs output corresponding to the different structural parameters considered.

The evolution of broadband SC spectra over the entire PCF length can be described from the spectral density plots (bottom rows) shown in Figs. 5 and 6. Since the pump source falls in the anomalous GVD regime of an each optimized PCF structure and when an ultrashort pulse transmits in this regime, the initial SC broadening is started with the self-phase modulation (SPM) and later more broadening is occurred through the soliton fission process. Solitons order ($N = \sqrt{L_{\mathrm{D}}/L_{\mathrm{NL}}}$) for all the proposed PCF structures can be calculated between 12 and 25 from the dispersion length, $L_{\mathrm{D}} = T_{\mathrm{P}^2}/|\beta_2|$ and the nonlinear length, $L_{\mathrm{NL}} = 1/\gamma \mathrm{P}$. In 10-mm-long PCF geometries, soliton fission occurs between 2 mm and 3 mm distance along the length of all the proposed structures. In the case of Fig. 5, if we observe the spectral density plots in bottom row, we can see that

soliton fission occurs around at 2 mm distance along the length of each optimized PCF. As a result of fission process, 14 to 25 fundamental solitons are induced owing to pulse envelop break up inside the optimized PCF geometries shown in Fig. 5. Fundamental solitons, which are induced after fission, are continuously red shifted yielding a number of spectral peaks in the spectra as a result of Raman induced frequency shift (RIFS). Solitons stop their red shifting movement due to spectral recoil effect (Biancalana et al. 2004) which occurs at 2nd ZDW of each GVD curve. However, according to the law of conservation of energy, a large red shifted dispersive wave (DW) emits owing to the presence of higher-oder dispersion terms after the 2nd ZDW of the each optimized structures where energy transfer occurs from soliton to DW by spectral recoil effect. This phenomena can clearly be seen in Figs. 5(e)-5(h), respectively. On the other hand, a blue shifted resonant narrow DW, which is nearly located around 1.9 μm, is observed as a result of shedding energy from the solitons due to the influence of same higher-order dispersion terms in the normal dispersion region before the 1st ZDW of each optimized structures. These phenomena can be clearly observed from the Figs. 5(e)-5(h), respectively.

Microstructured fibers made from ChG glasses with a periodic air-hole arrangements can be fabricated using the Stack-and-Draw method. This method is particularly suitable for the PCFs with a regular pitch. As an alternative to Stack-and-Draw method, the extrusion principle can also be employed to fabricate the PCFs made from soft glass material. Soft glasses made from ChGs can accept high dopant concentrations whcin helps to modify the optical and mechanical characteristics of these glasses more widely than silica glass. This is highly conducive to fabricate the PCFs with a more intricate microstructure incorporating a high refractive index contrast which results in a large nonlinear coefficient (Brilland et al. 2006).

4 Conclusions

We have numerically designed and modeled a number of 10-mm-long dispersion-engineered conventional hexagonal PCFs for ultrabroadband MIR region SC generation through the variations of their geometrical parameters Λ and d/Λ. The rigorous analysis through structural variations of microstructured fiber proposed in this paper revealed that it is possible to generate MIR SC broadening up to the lowest spanning of 8.5 μm to transparency limit of the GeAsSe material which is near to 14 μm by applying low input peak power between 3 kW and 4 kW with a tunable pump source which can be tunned between 2 μm and 4.3 μm. Initially, spectral broadening can be obtained up to 8.5 μm using a pump source at 3.2 μm for the PCF structure of $\Lambda = 2.4$ and d/$\Lambda = 0.45$ with a low input peak power of 3 kW. Subsequent spectral variations show that SC spectral spanning can be broadened up to 12.2 μm with the same pump and low peak power for the PCF structure of $\Lambda = 2.6$ and d/$\Lambda = 0.5$. To enhance the spectrum further in the MIR, next PCF structure optimized by increasing Λ to 2.7 μm while keeping pump and all other parameters same as applied before. By this design, spectral extension can be achieved up to 13 μm. However, a dip appears between 6 μm and 10 μm which belongs to the middle of the spectrum. Raising input peak power to 4 kW into this structure, spectral broadening can be predicted up to 13.5 μm covering the wavelength range 1.8–13.5 μm which is measured at -20 dB level from the peak

where long wavelength edge of the spectrum reached near to the transparency limit of the proposed ChG material. The SC broadening can be extended beyond 14 μm with further structural parameters variations which will induce more spectral dip into the SC spectrum with the same peak power applied and the input peak power has to be enhanced further to realized a SC output in similar spectral power level as compared to the earlier designs. The output SC broadening may be varied somewhat owing to the polarization perturbations of the fiber. The proposed broadband SC source, which is numerically designed based on traditional hexagonal PCF, would be highly suitable for MIR region SC generation and can be utilized for a variety of MIR region sensing and imaging applications.

5 ACKNOWLEDGEMENT

Funding for this research was provided by the Ministry of Higher Education (MOHE) under the grants GA 010-2014 (ULUNG) and the University of Malaya under the grants RP029B-15 AFR and RU001-2017. We would also like to thank the City, University of London for providing support for this work under the Newton Fund Grant IF026-2018.

References

1. Agrawal, G. P.: Nonlinear Fiber Optics 5th ed. (Academic, San Diego, California, 2013)
2. Aggarwal, I. D. and Sanghera, J. S.: Development and applications of chalcogenide glass optical fibers at NRL. J. Optoelectron. Adv. Mater. **4**(3), 665–678 (2002)
3. Al-Kadry, A., Amraoui, M. E., Messaddeq, Y., and Rochette, M.:Two octaves mid-infrared supercontinuum generation in As_2Se_3 microwires. Opt. Exp. **22**(25), 31131–31137 (2014)
4. Biancalana, F., Skryabin, D. V., and Yulin, V.: Theory of the soliton self-frequency shift compensation by resonant radiation in photonic crystal fibers. Physical Review E **70** 016615 (2004)
5. Brilland, L., Smektala, F., Renversez, G., Chartier, T., Troles, J., Nguyen, T. N., Traynor, N., and Monteville, A.: Fabrication of complex structures of Holey Fibers in chalcogenide glasses. Opt. Express **14** 1280–1285 (2006)
6. Cheng, T., Zhang, L., Xue, X., Deng, D., Suzuki, T., and Ohishi, Y.: Broadband cascaded four-wave mixing and supercontinuum generation in a tellurite microstructured optical fiber pumped at 2 μm. Opt. Express **23** 4125–4134 (2015)
7. Cheng, T., Nagasak, K., Tuan, T. H., Xue, X., Matsumoto, M., Tezuka, H., Suzuki, T., and Ohishi, Y.: Mid-infrared supercontinuum generation spanning 2 to 15.1 μm in a chalcogenide step-index fiber *Opt. Lett.* **41** 2117–2120 (2016)
8. Cregan, R. F., Mangan, B. J., Knight, J. C., Birks, T. A., Russell, P. S., Roberts, P. J., and Allan, D. C.: Single-mode photonic band gap guidance of light in air. Science **5433**, 1537–1539 (1999)
9. Domachuk, P., Wolchover, N. A., Cronin-Golomb, M., Wang, A., George, A. K., Cordeiro, C. M. B., Knight, J. C., and Omenetto, F. G.: Over 4000 nm bandwidth of Mid-IR supercontinuum generation in subcentimeter segments of highly nonlinear tellurite PCFs. Opt. Express **16** 7161–7168 (2008)
10. Dudley, J. M., Genty, G., and Coen, S.: Supercontinuum generation in photonic crystal fiber. Rev. Mod. Phys. **78**, 1135–1184 (2006)
11. Dudley, J. M. and Taylor, J. R.: Ten years of nonlinear optics in photonic crystal fiber. Nat. Photonics **3** 85–90 (2009)
12. Dupont, S., Petersen, C., Thøgersen, J., Agger, C., Bang, O., and Keiding, S. R.: IR microscopy utilizing intense supercontinuum light source. Opt. Express **20** 4887–4892 (2012)
13. Eggleton, B .J., Luther-Davies, B., and Richardson, K.: Chalcogenide photonics. Nat. Photonics **5** 141–148 (2011)

14. Fatome, J., Fortier, C., Nguyen, T. N., Chartier, T., Smektala, F., Messaad, K., Kibler, B., Pitois, S., Gadret, G., Finot, C., Troles, J., Desevedavy, F., Houizot, P., Renversez, G., Brilland, L., and Traynor, N.: Linear and nonlinear characterizations of chalcogenide photonic crystal fibers. J. Lightwave Technol. **27**(11), 1707–1715 (2009)
15. Gai, X., Han, T., Prasad, A., Madden, S., Choi, D. Y., Wang, R., Bulla, D., and Luther-Davies, B.: Progress in optical waveguides fabricated from chalcogenide glasses. Opt. Exp. **18**(25), 26635–26646 (2010)
16. Gao, W., Amraoui, M. E., Liao, M., Kawashima, H., Duan, Z., Deng, D., Cheng, T., Suzuki, T., Messaddeq, Y., and Ohishi, Y.: Mid-infrared supecontinuum generation in a suspended-core As_2S_3 chalcogenide microstructured optical fiber. Opt. Express **21** 9573–9583 (2013)
17. Habib, M. S., Markos, C., Bang, O., and Bache, M.: Soliton-plasma nonlinear dynamics in mid-IR gas-filled hollow-core fibers. Opt. Lett. **42** 2232–2235 (2017)
18. Hu, J., Menyuk, C. R., Shaw, L. B., Sanghera, J. S., and Aggarwal, I. D.: Maximizing the bandwidth of supercontinuum generation in As_2Se_3 chalcogenide fibers. Opt. Exp. **18**(3), 6722–6739 (2010)
19. Hudson, D. D., Mägi, E. C., Judge, A. C., Dekker, S. A., and Eggleton, B. J.: Highly nonlinera chalcogenide glass micro/nanofiber devices: Design, theory, and octave-spanning spectral generation. Opt. Commun. **285** 4660–4669 (2012)
20. Hudson, D. D., Antipov, S., Li, L., Alamgir, I., Hu, T., El-Amraoui, M., Messaddeq, Y., Rochette, M., Jackson, S. D., and Fuerbach, A.: Toward all-fiber supercontinuum spanning the mid-infrared. Optica **4** 1163–1166 (2017)
21. Karim, M. R., Rahman, B. M. A., and Agrawal, G. P.: Dispersion engineered $Ge_{11.5}As_{24}Se_{64.5}$ nanowire for supercontinuum generation: A parametric study. Opt. Exp. **22**(25), 31029–31040 (2014)
22. Karim, M. R., Rahman, B. M. A., Azabi, Y. O., Agrawal, A., and Agrawal, G. P.: Ultra-broadband mid-infrared supercontinuum generation through dispersion engineering of chalcogenide microstructured fibers. J. Opt. Soc. Am. B **32** 2343–2351 (2015)
23. Karim, M. R., Ahmad, H., and Rahman, B. M. A.: Design and modeling of dispersion-engineered all-chalcogenide triangular-core fiber for mid-infrared-region supercontinuum generation, J. Opt. Soc. Am. B **35** 266–275 (2018)
24. Knight, J. C. and Russell, P. S. J.: Photonic crystal fibers: New ways to guide light. Science **296** 276–277 (2002)
25. Knight, J. C., Birks, T. A., Russell, P. S., and Atkin, D. M.: All-silica single-mode optical fiber with photonic crystal cladding. Opt. Lett. **21** 1547–1549 (1996)
26. Kubat, I., Agger, C. S., Møller, U., Seddon, A. .B, Tang, Z., Sujecki, S., Benson, T. M., Furniss, D., Lamarini, S., Scholle, K., Fuhrberg, P., Napier, B., Farries, M., Ward, J., Moselund, P. M., and Bang, O.: Mid-infrared supercontinuum generation to 12.5 μm in large NA chalcogenide step-index fibers pumped at 4.5μm. Opt. Express **22** 19169–19182 (2014)
27. Kubat, I. and Bang, O.: Multimode supercontinuum generation in chalcogenide glass fibres. Opt. Express **24** 2513–2526 (2016)
28. Liao, M., Qin, G., Yan, X., Suzuki, T., and Ohishi, Y.: A Tellurite nanowire with long suspended struts for low-threshold single-mode supercontinuum generation. J. Lightwave Technol. **29** 194–199 (2011)
29. Liu, L., Cheng, T., Nagasaka, K., Tong, H., Qin, G., Suzuki, T., and Ohishi, Y.: Coherent mid-infrared supercontinuum generation in all-solid chalcogenide microstructured fibers with all-normal dispersion. Opt. Lett. **41** 392–395 (2016)
30. Magi, E, C., Fu, L. B., Nguyen, H. C., Lamont, M. R. E., Yeom, D. I., and Eggleton, B. J.: Enhanced Kerr nonlinearity in sub-wavelength diameter As_2Se_3 chalcogenide fiber tapers. Opt. Express **15** 10324–10329 (2007)
31. Ma, P., Choi, D. Y., Yu, Y., Gai, X., Yang, Z., Debbarma, S., Madden, S., and Luther-Davies, B.: Low-loss chalcogenide waveguides for chemical sensing in the mid-infrared. Opt. Exp. **21**(24), 29927–29937 (2013)
32. Markos, C. and Bang, O.: Nonlinear label-free biosensing with high sensitivity using As_2S_3 chalcogenide tapered fiber. J. Lightwave Technol. **33**(13) 2892–2898 (2015)
33. Markos, C., Travers, J. C., Abdolvand, A., Eggleton, B. J., and Bang, O.: Hybrid photonic-crystal fiber. Rev. Mod. Phys. **89**(4) 045003 (2017)
34. Møller, U., Yu, Y., Kubat, I., Petersen, C. R., Gai, G., Brilland, L., Mechin, D., Caillaud, C., Troles, J., Luther-Davies, B., and Bang, O.: Multi-milliwatt mid-infrared supercontinuum generation in a suspended core chalcogenide fiber. Opt. Exp. **23**(3), 3282–3291 (2015)

35. Ou, H., Dai, S., Zhang, P., Liu, Z., Wang, X., Chen, F., Xu, H., Luo, B., Huang, Y., and Wang, R.: Ultrabroad supercontinuum generated from a highly nonlinear Ge–Sb–Se fiber. Opt. Lett. **41** 3201-3504 (2016)
36. Petersen, C. R., Møller, U., Kubat, I., Zhou, B., Dupont, S., Ramsay, J., Benson, T., Sujecki, S., Abdel-Moneim, M., Tang, Z., Furniss, D., Seddon, A., and Bang, O.: Mid-infrared supercontinuum covering the 1.4-13.3 μm molecular fingerprint region using ultra-high NA ChG step-index fiber. Nat. Photonics **8** 830–834 (2014)
37. Petersen, C. R.,Prtljaga, N., Farries, M., Ward, J., Napier, B., Lloyd, G. R., Nallala, J., Stone, N., and Bang, O.: Mid-infrared multispectral tissue imaging using a chalcogenide fiber supercontinuum source. Opt. Lett. **43** 999–1002 (2018)
38. Petersen, C. R., Engelsholm, R. D., Markos, C., Brilland, L., Caillaud, C., Troles, J., and Bang, O.: Increased mid-infrared supercontinuum bandwidth and average power by tapering large-mode-area chalcogenide photonic crystal fibers. Opt. Express 25 15336–15348 (2017)
39. Qin, G., Yan, X., Kito, C., Liao, M., Chaudhari, C., Suzuki, T., and Ohishi, Y.: Ultrabroadband supercontinuum generation from ultraviolet to 6.28 μm in a fluoride fiber. Appl. Phys. Lett. **95**(16), 161103 (2009)
40. Rahman, B. M. A. and Davies, J. B.: Finite-element solution of integrated optical waveguides. J. Lightwave Technol. **2**, 682–688 (1984)
41. Saini, T. S., Kumar, A., and Sinha, R. K.: Broadband mid-infrared supercontinuum spectra spanning 2-15 μm using As_2Se_3 chalcogenide glass triangular-core graded-index photonic crystal fiber. J. Lightw. Technol. **33** 3914–3920 (2015)
42. Sanghera, J., Florea, C., Shaw, L., Pureza, P., Nguyen, V., Bashkansky, M., Dutton, Z., and Aggarwal, I. D.: Non-linear properties of chalcogenide glasses and fibers. J. Non-Cryst. Solids **354** 462 (2008)
43. Schliesser, A., Picque, N., and Haensch, T. W.: Mid-infrared frequency combs. Nat. Photonics **6** 440–449 (2012)
44. Seddon, A. B., Napier, B., Lindsay, I., Lamrini, S., Moselund, P. M., Stone, N., Bang, O.: Mid-infrared Spectroscopy/Bioimaging: Moving toward MIR optical biopsy. Laser Focus World **52**(2) 50–53 (2016)
45. Shaw, L. B., Gattass, R. R., Sanghera, J. S., and Aggarwal, I. D.: All-fiber mid-IR supercontinuum source from 1.5 to 5 μm. Proc. SPIE **7914** (2011)
46. Swiderski, J. and Michalska, M.: High-power supercontinuum generation in a ZBLAN fiber with very efficient power distribution toward the mid-infrared. Opt. Lett. **39** 910–913 (2014)
47. Tajima, K., Zhou, J., Nakajima, K., and Sato, K.: Ultra low loss and long length photonic crystal fiber. J. Lightwave Technol. **22**(1) 7–10 (2004)
48. Tang, Y., Wright, L. G., Charan, K., Wang, T., Xu, C., and Wise, F. W.: Generation of intense 100-fs solitons tunable from 2 to 4.3 μm in fluoride fiber. Optica **3** 948–951 (2016)
49. Toupin,P., Brilland, L., Troles, J., and Adam, J. -L.: Small core Ge-As-Se microstructured optical fiber with single-mode propagation and low optical losses. Opt. Mater. Express **2** 1359–1366 (2012)
50. Wang, T., Gai, X., Wei, W., Wang, R., Yang, Z., Shen, X., Madden, S., and Luther-Davies, B.: Systematic z-scan measurements of the third order nonlinearity of chalcogenide glasses. Opt. Mater. Express **4** 1011–1022 (2014)
51. Wei, C., Zhu, X., Norwood, R. A., Seng, F., and Peyghambarian, N.: Numerical investigation on high power mid-infrared supercontinuum fiber lasers pumped at 3 μm. Opt. Exp. **21**(24), 29488–29504 (2013)
52. Xing, S., Grassani, D., Kharitonov, S., Billat, A., and Bres, C-S.: Characterization and modeling of microstructured chalcogenide fibers for efficient mid-infrared wavelength conversion. Opt. Express **24** 9741–9750 (2016)
53. Xing, S., Grassani, D., Kharitonov, S., Brilland, L., Caillaud, C., Troles, J., and Bres, C-S.: Mid-infrared continuous-wave parametric amplification in chalcogenide microstructured fibers. Optica **4** 643–648 (2017)
54. Yu, Y., Gai, X., Zhai, C., Qi, S., Guo, W., Yang, Z., Wang, R., Choi, D., Madden, S., and Luther-Davies, B.: 1.8-10 μm mid-infrared supercontinuum generation in a step-index chalcogenide fiber using low peak pump power. Opt. Lett. **40**(6), 1081–1084 (2015)
55. Zhao, Z., Wu, X., Wang, W., Pa, Z., Liu, Z., Zhang, P., Shen, X., Nie, Q., Dai, S., and Wang, R.: Mid-infrared supercontinuum covering 2–16 μm in a low-loss telluride single-mode fiber. Laser Photonics Rev. **2** 1700005 (2017)